Asian Journal of Chemistry; Vol. 37, No. 3 (2025), 715-721

ASIAN JOURNAL OF CHEMISTRY

https://doi.org/10.14233/ajchem.2025.33300

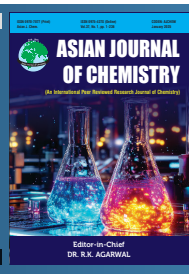

Influence of Surfactant Trilaurin Concentration on Synthesis of Hydroxyapatite by Ultrasound Assisted Biomimetic Method

E. SATHYA and V. COLLINS ARUN PRAKASH*

PG & Research Department of Chemistry, Sacred Heart College (Autonomous) (Affiliated to Thiruvalluvar University, Serkkadu), Tirupattur-635601, India

*Corresponding author: Fax: +91 4179 226423; Tel: +91 4179 225503; E-mail: collinsnanobio@gmail.com

Received: 30 December 2024; *Accepted*: 15 February 2025; *Published online*: 28 February 2025; AJC-21929

In present study, three different concentrations of a novel surfactant trilaurin has been reported using ultrasound method for synthesizing hydroxyapatite (HAP) powders in presence of the simulated body fluid (SBF) as a solvent in order to investigate the apoptotic cell response. The materials were characterized with FTIR, XRD, SEM, TEM, TGA, BET techniques as well as cytotoxicity (MTT assay) using appropriate cell line. The nanoHAP was characterized for their size and morphology by HRSEM and HRTEM techniques, respectively and were found to have a nanorod like morphology with an average length of 50 nm. The results also validates the cytotoxicity which shows good biocompatibility of nanoHAP powders. The synthesized HAP powders was found to possess improved and uniform size distribution due to the use of non-ionic natural organic modifier (trilaurin). The concentration of trilaurin influences the morphology of the synthesized HAP powders.

Keywords: Hydroxyapatite, Ultrasound, Trilaurin, Nanorods, Apoptosis, Simulated body fluid.

INTRODUCTION

Among biomaterials, hydroxyapatite (HAP) is the most commonly used and essentially produced. Because of its slow degradability, lack of inflammation and sustained stability, hydroxyapatite is a good choice for bone substitutes [1-3]. Additionally, it can be used for implant coating, drug delivery and orthopaedic applications [4-6]. Due to its structural and chemical similarities to the mineral phase of human bones and teeth, HAP, a well-known bioceramic material, might be widely considered for its good biocompatibility [7,8]. To enhance the bioactive qualities of HAP specifically in orthopaedic applications, it is employed in synthetic and sterilized form. The significance of HAP has prompted substantial studies in a variety of fields, including its application as a biological or industrial substance [9-12] and the physico-chemical mechanisms underlying its synthesis.

To achieve this, simulated body fluid (SBF) is utilized as a medium, originally developed by Kokubo *et al*. [13], with ionic concentrations that match those of human blood plasma. This approach aims to reduce the particle sizes and narrow size distribution while enhancing bioactivity. Recent studies [14-16] have proven the successful biomimetic preparation of HAP employing 1.5 times concentrated SBF using ultrasonic irradiation. Since, the ionic intensity of SBF at physiological temperature and pH could greatly affect the crystallinity of HAP behaves. Various synthesis processes are employed to achieve the final stoichiometry, crystal size control, prevention of agglomeration, phase purity, form characteristics and sinterability of the final powder. A further key issue for the biomedical field is the continued rapid development of HAP with an affordable and reliable method to scale-up proficiency [17,18].

For the synthesis of hydroxyapatite, synthetic processing techniques are taken into account. The main drawbacks of high temperature processes, such as solid state and combustion procedures, include the tendency for non-stoichiometric products, the development of byproducts and the presence of contaminants. Wet chemical techniques are used to quickly prepare pure HAP at lower processing temperatures in order to get around these disadvantages. Additionally, advanced approaches make it simpler to manage morphology, particle shape and size distribution, which affect medical use and implementation [19,20].

Utilizing wet chemical methods, several different types of chemical synthesis techniques, including hydrothermal [21], sol-gel [22], sonochemical [23], precipitation [24], microwave [25], microemulsion [26], ball milling [27] and surfactant assisted approach [28], have been proposed for the synthesis of HAP nanopowders.

According to recent reports, the sonochemical approach holds the most promising method for producing hydroxyapatite with unique morphologies and characteristics. The generation of acoustic cavitation, ongoing bubble formation, expansion and implosive collapse in a liquid depends on the reaction sparked by strong ultrasonic radiation [29-31]. Moreover, it significantly speeds up the rate of the reaction between calcium and phosphate precursors [32,33]. Without the use of surfactants, the aggregation of particles could not be prevented. The surfactant also lowers the size of the crystals and the particles. Lipid-based nanocarriers have also been widely used to increase the emulsification and bioavailability of drug delivery. Various organic modifiers, such as PEG [34-36], SDS [37], CTAB [38-40] and PVA [41,42] have also been reported in the literature.

Trilaurin, a novel lipid-based surfactant, was selected as a natural organic modifier since it is biodegradable. Trilaurin is a lipid based surfactant have emerged a promising strategy for improved therapaeutic compound oral bioavailability [43]. Here, a naturally derived organic modifier approach that uses ultrasound to develop hydroxyapatite (HAP) in simulated body fluid (SBF) at different trilaurin concentrations. The nanoHAP was characterized to assess the surface morphology as well as their pore size.The results were compared with different concentrations of trilaurin, a synthetically produced HAP, utilizing an ultrasonic technique in SBF media. Moreover, DAPI staining was used to examine the apoptotic potential and fluorescent staining images show a significant alteration in cell line morphology.

EXPERIMENTAL

Hydrochloric acid (HCl) and dipotasium hydrogen phosphate trihydrate ($KHPO_4{\cdot}3H_2O$) were purchased from Merck Co. Ltd. (Germany). Ethanol (99.8%), tris(hydroxyl methyl)-aminomethane (Tris), sodium hydroxide, sodium chloride, potassium chloride, sodium bicarbonate, magnesium chloride hexahydrate, calcium chloride and sodium sulfate anhydrous, calcium nitrate tetrahydrate, trilaurin (TL) and diammonium hydrogen phosphate were purchased from Sigma-Aldrich, USA. All the chemicals were of analytical grade and used without further purification. Deionized water was used throughout the experiments.

Synthesis of simulated body fluid (SBF): SBF solution was prepared according to the reported method [43,44] by dissolving suitable quantities of the chemicals containing double deionized water (700 mL), which was continuously stirred at 37 ºC followed by the addition of reagents in order as mentioned in Table-1. After that, about 40 mL of HCl was used for pH adjustments. A 15 mL of HCl was added before adding $CaCl_2$ and the remaining HCl was added during titration. Particularly, the 8th reagent in Table-1, tris [$(CH_2OH)_3CNH_2$)] was added in dropwise to avoid an increase in pH of the solution. The physiological temperature of the solution was kept constant as 37 ºC, followed by titrating with HCl *vs.* Tris buffer to adjust the pH to 7.4. The ionic concentration of the SBF solutions were compared with human blood plasma as given in Table-1.

Synthesis of HAP powder using trilaurin: Calcium nitrate (0.5 M) and $KHPO_4{\cdot}3H_2O$ (0.3 M) were dissolved separately in 20 mL of SBF for the synthesis of HAP and a stoichiometric ratio of 1.67 was maintained. Thereafter, dropwise addition of two solutions were prepared while stirring continuously for 1 h. The pH of the solution was then increased to 10 using aqueous NH_3 and then stirred for 2 h. The obtained white suspension underwent 1 h long ultrasonic treatment. The resultant precipitate was then aged for 24 h and cleaned three times with ethanol and water. In order to obtain pure HAP, the washed samples were finally dried for 3 h at 100 ºC in an oven, followed by calcination and sintering. Trilaurin was used in three different concentrations using the same process. The synthesis was carried out using three different concentration of trilaurin.

RESULTS AND DISCUSSION

FT-IR spectral studies: FTIR spectra for HAP and trilaurin assisted HAP are shown in Fig. 1. The characteristic absorption peaks obtained for HAP can be assigned as OH, CO_3^{2-} and PO_4^{3-} groups. The characteristic band at 955 cm^{-1} has been ascribed to ν_1(PO) symmetrical stretching modes, whereas the ranges of 1017 cm^{-1} have been assigned as ν_3(PO) antisymmetrical stretching vibration modes of phosphate group. At 407 cm^{-1} ν_2(O-P-O) bending modes of phosphate group is obtained. The presence of the ν_4 bending mode of the phosphate group obtained in the range of 558 cm^{-1}. The stretching vibrations obtained at the wavenumber 3568 cm^{-1} and bending vibration mode at 633 cm^{-1} were corresponds to the hydroxyl group [45,46]. The band obtained at the wavenumber 1460 cm^{-1} are assigned as carbonate group which was obtained from SBF & atmosphere during precipitation process (Table-2).

XRD studies: Fig. 2a-d demonstrate the XRD patterns of HAP with trilaurin at varied concentrations. The purity of the obtained products was examined by XRD pattern. Fig. 2a indicates the XRD patterns of HAP nanoparticles and all the diffraction peaks can be well assigned to hexagonal phase, which are known the HAP hexagonal phase (ICDD card # 09-0432) and space group of *P*63/*m*. From Fig. 2a-d, it is obvious

TABLE-1
IONIC CONCENTRATION OF THE SBF SOLUTIONS AND THEIR COMPARISON WITH HUMAN BLOOD PLASMA

Solutions	Concentrations (mol/m^3)									
	Na^+	K^+	Mg^{2+}	Ca^{2+}	Cl^-	HCO^{3-}	HPO_4^{2-}	PO_4^{3-}	SO_4^{2-}	Ca/P
HBP (mM)	142.0	5.0	1.5	2.5	103.0	27.0	1.0	–	0.50	2.5
SBF (mM)	141.5	5.0	1.5	2.5	124.5	27.0	1.0	–	0.50	2.5
1.5SBF (mM)	212.3	7.5	1.5	3.8	186.8	40.5	1.5	–	0.75	–

TABLE-2
WAVENUMBER (cm^{-1}) REGIONS FOR HYDROXYAPATITE

Sample	Free water	$\nu_3 CO_3^{2-}$	$\nu_{3c} PO_4^{3-}$	$\nu_4 PO_4^{3-}$	$\nu_2 PO_4^{3-}$	$\nu_1 PO_4^{3-}$	$\nu_3 PO_4^{3-}$	$\nu_4 CO_3^{2-}$
HAP	3566	1459	1018	600,588	471	952	634	421
0.1 g-trilaurin	3572	1466	1019	602,556	471	959	621	421
0.3 g-trilaurin	3572	1453	1018	602,562	471	951	634	421
0.5 g-trilaurin	3568	1460	1017	600,558	407	955	633	407

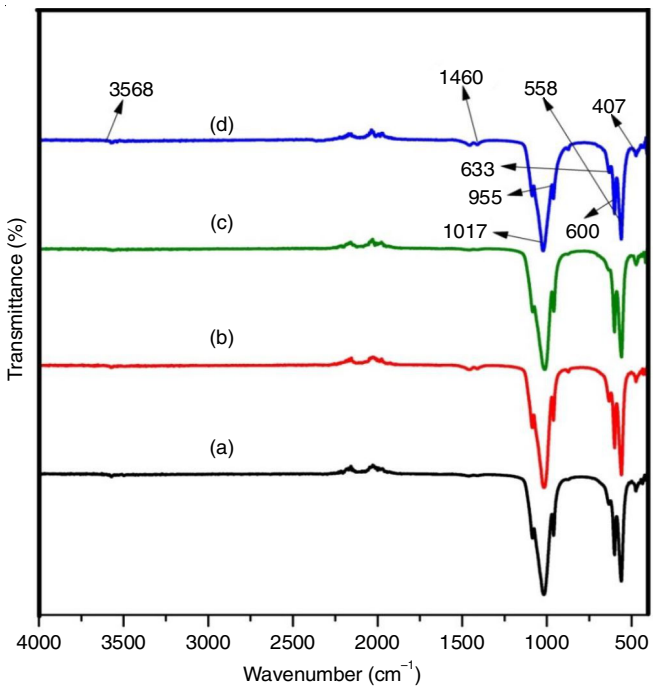

Fig. 1. FTIR spectra of HAP sample obtained in SBF (a) HAP, (b) trilaurin-0.1 g, (c) trilaurin-0.3 g and (d) trilaurin-0.5 g

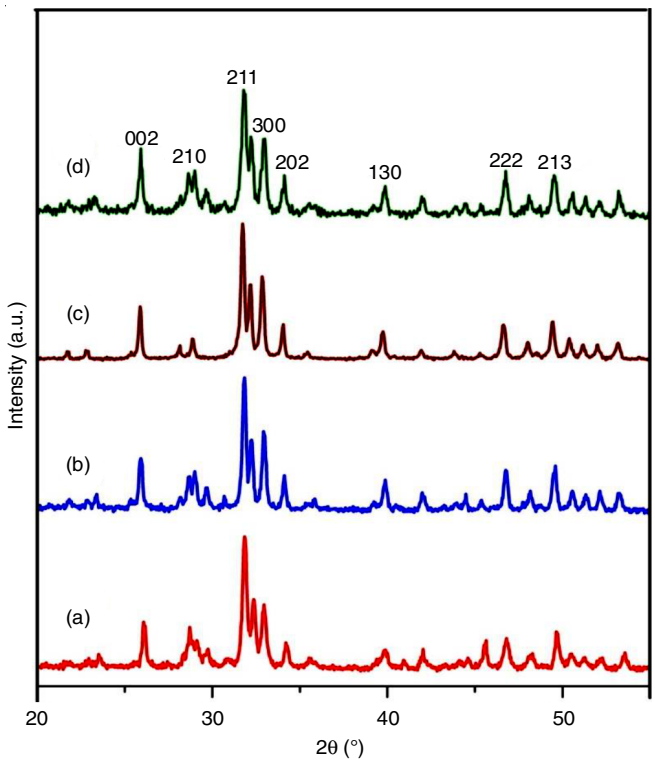

Fig. 2. XRD patterns of HAP sample obtained in SBF (a) HAP, (b) trilaurin-0.1 g, (c) trilaurin-0.3 g and (d) trilaurin-0.5 g

that the intensity of (002) planes are increased with increase in trilaurin concentration, which strongly suggests that increase in intensity leads to increase in crystallinity with respect to the other system of the as-synthesized HAP powder. The average crystallite size of blank HAP, 0.1 g trilaurin, 0.3 g trilaurin and 0.5 g trilaurin calculated using Debye-Scherrer's formula was 24, 20, 28 and 30 nm, respectively. The crystallite size is considerably increased with increase in trilaurin concentration. Smaller the FWHM values, higher the grain size [47] and the calculated XRD parameters are tabulated in Table-3.

TABLE-3
DIFFRACTION DATA FOR HAP AND TL ASSISTED HAP AT VARIED CONCENTRATIONS

Sample conditions	Plane	2θ (°)	Line width (FWHM)	Grain size (nm)	d-spacing (nm)
HAP	211	31	0.35	24	0.28
Trilaurin-0.1 g	211	31	0.30	20	0.28
Trilaurin-0.3 g	211	31	0.27	28	0.28
Trilaurin-0.5 g	211	31	0.24	30	0.28

SEM studies: The microstructural characteristics of the as synthesized HAP powders are investigated by SEM analysis. It is well-known that several factors influences the particle size and morphology of trilaurin assisted HAP. However, Fig. 3a-d shows the morphological images of the resultant nanostructure at different trilaurin concentrations. During precipitation in SBF solvent, the ions present in SBF induces the formation of nanosized HAP at different concentration of trilaurin. In Fig. 3a, the HRSEM obtained for HAP is spherical in shape, whereas Fig. 3b indicates 0.1g trilaurin the observed morphology is fully spherical. In Fig. 3c, the spherical morphology starts to elongates into rod. Finally, in Fig. 3d, particles are completely converted into rod like morphology. It is concluded that using SBF by varying trilaurin concentration, the morphological changes are observed.

HRTEM analysis: As given in Fig. 4a-b, the HAP nanoparticles was studied using HRTEM having an individual particle size in the range of 10 nm. TEM image shows particles are nearly similar in shape and interconnected particles with voids confirms the presence of separated particles. During ultrasound irradiation, as the sound waves passed to the sample the nano-HAP are arranged quickly into matrix without being separated into discrete nanoparticles. In Fig. 4c, SAED pattern with bright ring with spots indicates the crystallinity in contrast to the bulk apatite [48]. The *d*-spacing value obtained in lattice fringes of Fig. 4b-e correlates with the XRD. The trilaurin assisted HAP shows rod shaped morphologies and blank HAP shows spherical shaped morphology [49,50].

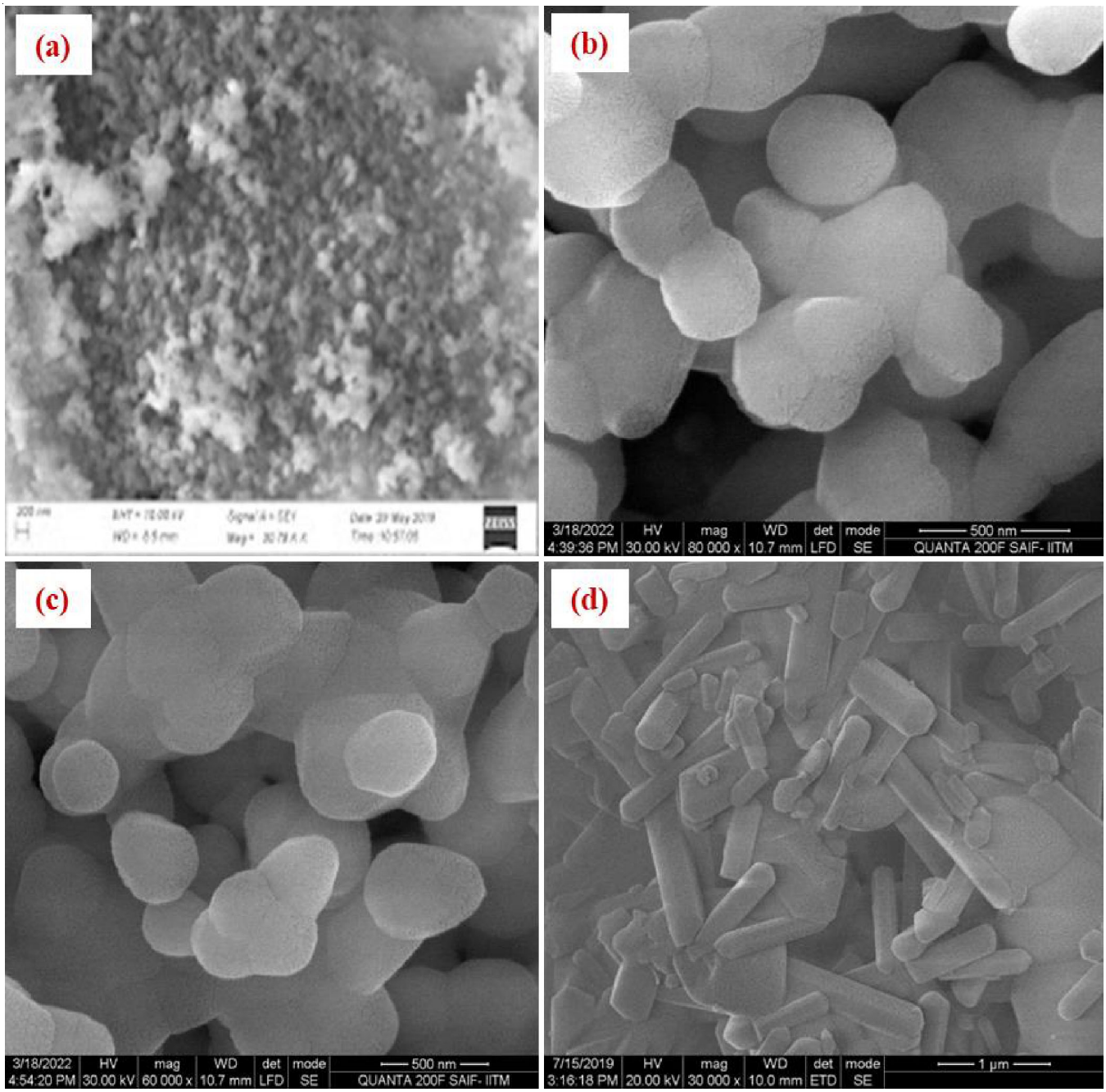

Fig. 3. SEM micrograph for (a) HAP, (b) trilaurin-0.1 g, (c) trilaurin-0.3 g and (d) trilaurin-0.5 g

Thermal studies: TG curves were recorded for the as synthesized HAP and different concentration of trilaurin assisted nanoHAP powders in the temperature range of 50-970 ºC. The thermal stability of the prepared samples was analyzed through thermogravimetric analysis are shown in Fig. 5a-d as per the observed from the HAP and TL-HAP samples, weight loss occurs in two stages: the first weight loss at 135 ºC due to the evaporation of absorbed water [51]. There is huge weight loss is observed at Fig. 5a-d samples at second stage in the region of 200-500 ºC is due to removal of lattice water [52]. On the contrary, the sudden weight loss occurs between 600-900 ºC at is due to thermal degradation of carbonate ions bound to HAP [53].

BET analysis: Nitrogen adsorption-desorption isotherm measurements were used to analyse the surface features of HAP samples; the results are displayed in Fig. 6. A Type II isotherm with a P/P_0 value between 0.8 and 0.9 [54] is shown in Fig. 6a, which suggests the formation of rod-shaped aggregates with large pores. By looking at the BJH plot, the pore radius of the as-synthesized HAP sample was determined using the desorption curve. The surface area of the trilaurin-assisted HAP sample, as determined by BET, is 11.19 $m^2 g^{-1}$.

Application of nano HAP powder

Fluorescence staining test: The morphological changes that takes place were detected *via* a fluorescence staining images

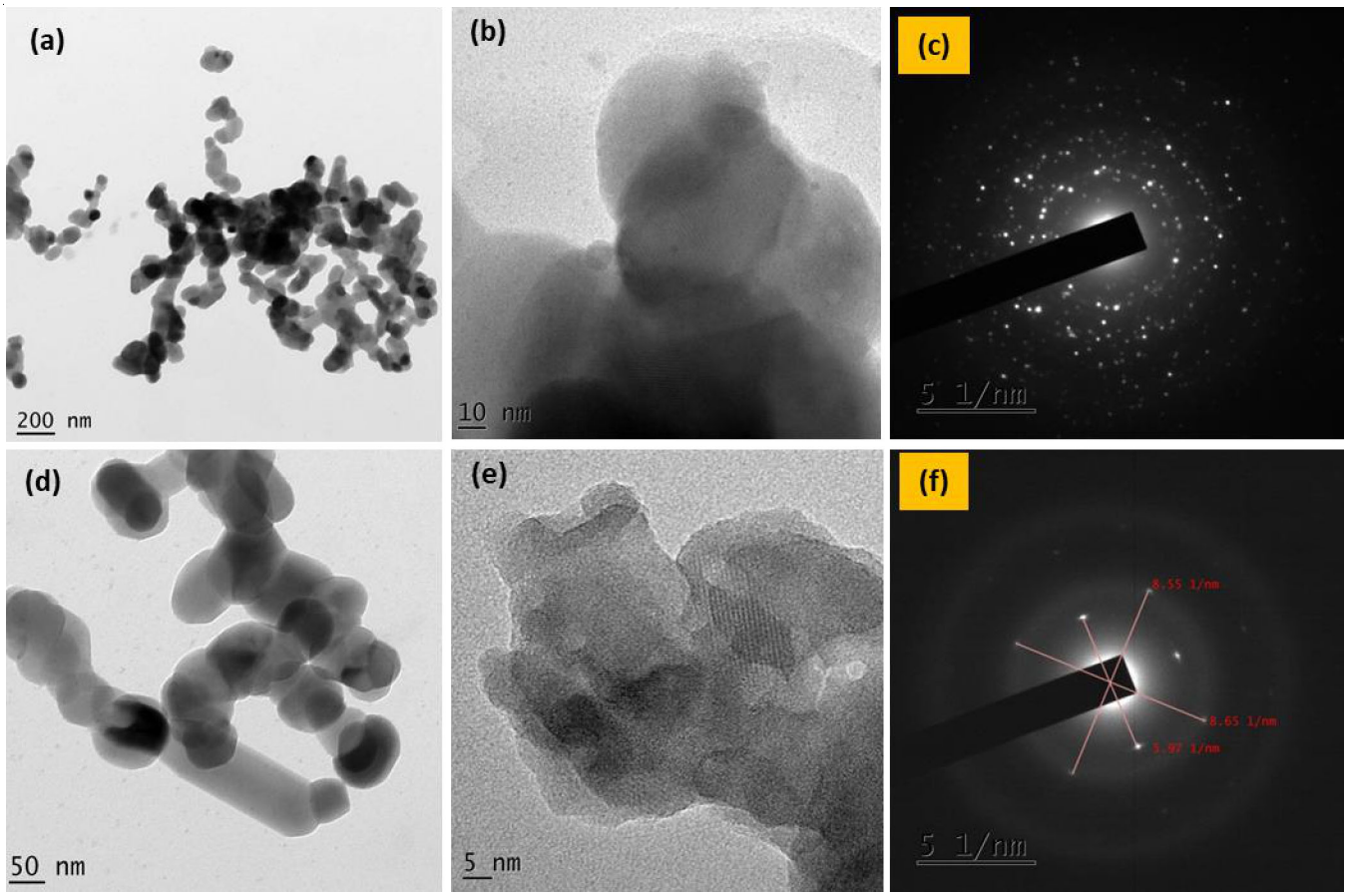

Fig. 4. HRTEM images for (a) HAP, (b) lattice fringes for HAP, (c) SAED pattern for HAP, (d) trilaurin, (e) lattice fringes for trilaurin and (f) SAED pattern for trilaurin

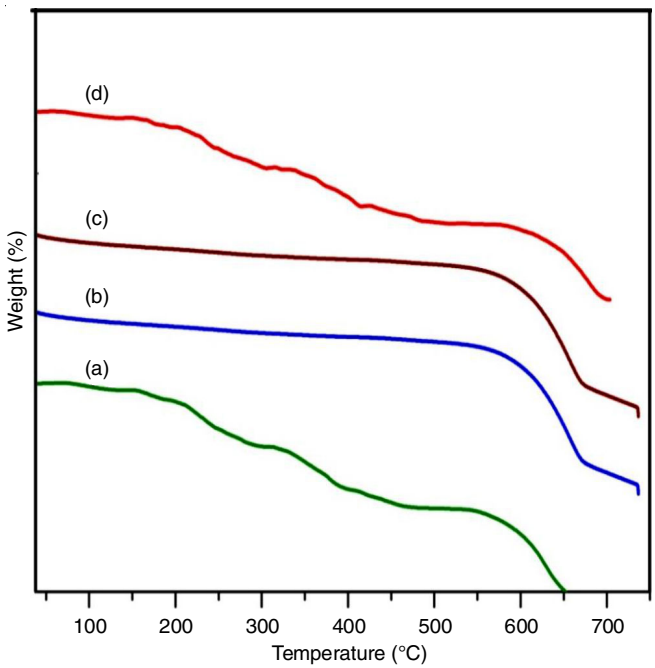

Fig. 5. Thermograms of (a) HAP, (b) trilaurin-0.1 g, (c) trilaurin-0.3 g and (d) trilaurin-0.5 g

as shown in Fig. 7a-b. In Fig. 7a for the untreated samples, the DAPI (4,6-diamidino-2-phenylindole) staining maintains the morphology of normal MCF-7 cell line, which includes intact nuclear structure. The MCF-7cell line is treated with trilaurin-HAP shows the change in morphology, which indicates that the apoptosis induction ability of trilaurin assisted HAP has been enhanced (Fig. 7b). Apoptosis is the cell death that occurs when there is a characteristic change in morphology of the cells. Using DAPI staining, the cells can be differentiated from apoptotic cells to normal cells [55-57].

Conclusion

In this work, trilaurin was synthesized at varying concentration using the ultrasound method in order to develop hydroxyapatite (HAP). The results shows that the unit cell volume, crystallite size and lattice parameters are significantly by increased trilaurin concentration. HAP powders with rod like morphology were successfully synthesized ultrasound method in the presence of trilaurin as organic modifier possessing excellent dispersing ability. The XRD studies affirmed that the nanoHAP possess hexagonal structure without an impurity phase. The XRD and HRSEM studies conclusively show the decrease in crystal size, the variation in surface morphology. TG analysis proves the high thermal stability of the synthesized nanoHAP, whereas the HRTEM image provides information about the nanopowders size of the samples. The apoptotic activity is induced by fluorescence staining assay using MCF-7 cell line.

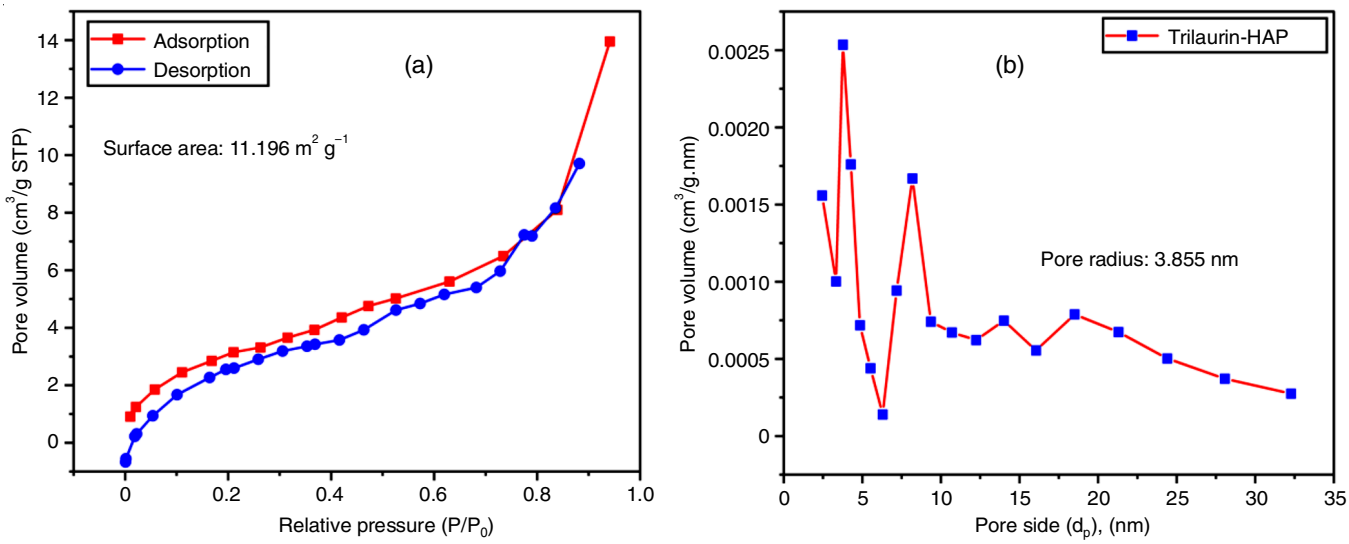

Fig. 6. (a) Nitrogen adsorption-desorption isotherm of HAP-trilaurin and (b) pore size distribution of HAP-trilaurin sample

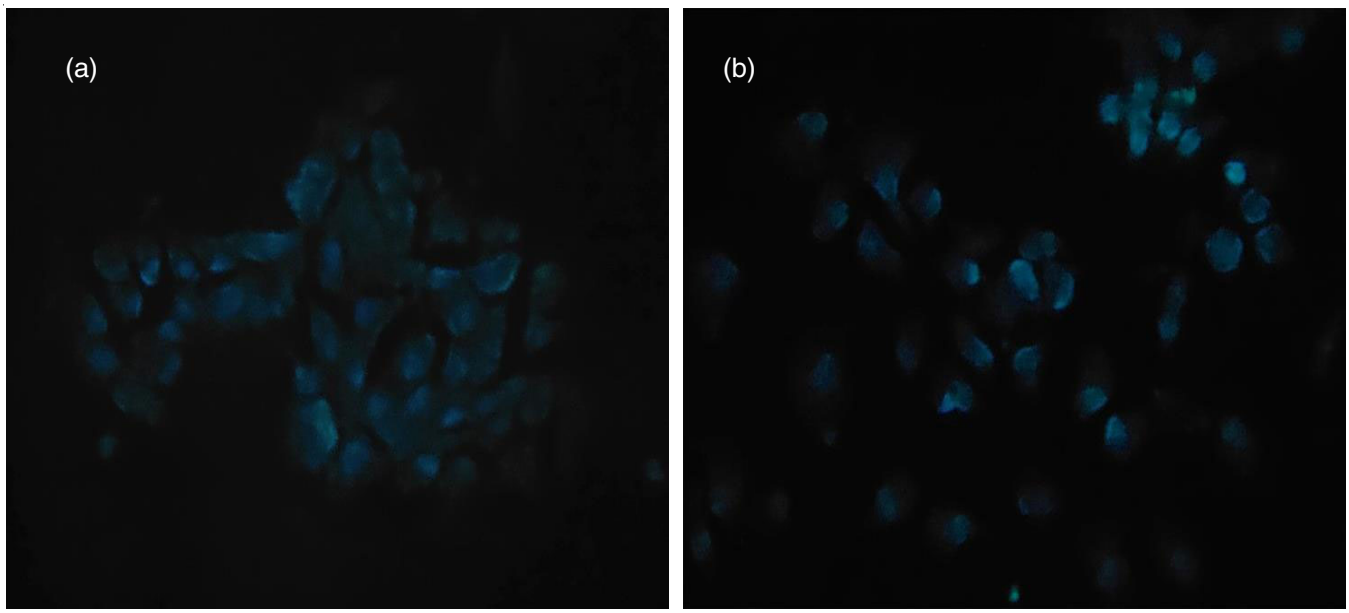

Fig. 7. Fluorescence images obtained on (a) untreated HAP and (b) treated with trilaurin-nano HAP

ACKNOWLEDGEMENTS

One of the authors (E. Sathya) thanks Fr. Carreno Research Grant, Sacred Heart College (Autonomous) Tirupattur, India for the financial assistance through received under "Fr. Carreno Research Grant" (SHC/Fr. Carreno Research Grant/2022/02).

CONFLICT OF INTEREST

The authors declare that there is no conflict of interests regarding the publication of this article.

REFERENCES

1. T. Markovich, D. Andelman and R. Podgornik, *Langmuir*, **33**, 34 (2017); https://doi.org/10.1021/acs.langmuir.6b03186.
2. A. Zaharia, V. Musat, E.M. Anghel, I. Atkinson, O.-C. Mocioiu, M. Busilă and V.G. Plescan, *Ceram. Int.*, **43**, 11390 (2017); https://doi.org/10.1016/j.ceramint.2017.05.346
3. F. Miculescu, A. Mocanu, G. Stan, M. Miculescu, A. Maidaniuc, A. Cîmpean, V. Mitran, S. Voicu, T. Machedon-Pisu and L. Ciocan, *Appl. Surf. Sci.*, **438**, 147 (2017); https://doi.org/10.1016/j.apsusc.2017.07.144
4. A. Szczes, L. Holysz and E. Chibowski, *Adv. Colloid Interface Sci.*, **249**, 321 (2017); https://doi.org/10.1016/j.cis.2017.04.007
5. A. Wang, H. Yin, D. Liu, H. Wu, M. Ren, T. Jiang, X. Cheng and Y. Xu, *Mater. Lett.*, **61**, 2084 (2007); https://doi.org/10.1016/j.matlet.2006.08.019
6. M. Aminzare, A. Eskandari, M.H. Baroonian, A. Berenov, Z. Razavi Hesabi, M. Taheri and S.K. Sadrnezhaad, *Ceram. Int.*, **39**, 2197 (2013); https://doi.org/10.1016/j.ceramint.2012.09.023
7. Y. Xu, T. Lu, F. He, N. Ma, J. Ye and T. Wu, *ACS Biomater. Sci. Eng.*, **4**, 3154 (2018); https://doi.org/10.1021/acsbiomaterials.8b00697
8. J.C. Elliott, Structure and Chemistry of the Apatites and Other Calcium Orthophosphates, Elsevier Science: The Netherlands (1994).
9. S. Koutsopoulos and E. Dalas, *Langmuir*, **16**, 6739 (2000); https://doi.org/10.1021/la000057z
10. S. Koutsopoulos and E. Dalas, *J. Colloid Interface Sci.*, **231**, 207 (2000); https://doi.org/10.1006/jcis.2000.7144

11. S. Koutsopoulos and E. Dalas, *Langmuir*, **17**, 1074 (2001); https://doi.org/10.1021/la000820p
12. H. Tanaka, K. Miyajima, M. Nakagaki and S. Shimabayashi, *Chem. Pharm. Bull. (Tokyo)*, **37**, 2897 (1989); https://doi.org/10.1248/cpb.37.2897
13. T. Kokubo, H. Kushitani, S. Sakka, T. Kitsugi and T. Yamamuro, *J. Biomed. Mater. Res.*, **24**, 721 (1990); https://doi.org/10.1002/jbm.820240607
14. H. Qu and M. Wei, *J. Biomed. Mater. Res. Part B Appl. Biomater.*, **87**, 204 (2008); https://doi.org/10.1002/jbm.b.31096
15. N. Arabi and A. Zamanian, *Biotechnol. Appl. Biochem.*, **60**, 573 (2013); https://doi.org/10.1002/bab.1120
16. A. Zamanian, S. Farhangdoust, M. Yasaei, M. Khorami and M. Hafezi, *Int. J. Appl. Ceram. Technol.*, **11**, 12 (2014); https://doi.org/10.1111/ijac.12031
17. E. Riman Richard, W. Suchanek, K. Byrappa, C. Chen, P. Shuk and C.S. Oakes, *Solid State Ion.*, **151**, 393 (2002); https://doi.org/10.1016/S0167-2738(02)00545-3
18. D. Liu, Q. Yang, T. Troczynski and W. Tseng, *Biomaterials*, **23**, 1679 (2002); https://doi.org/10.1016/S0142-9612(01)00295-2
19. A. Yelten-Yilmaz and S. Yilmaz, *Ceram. Int.*, **44**, 9703 (2018); https://doi.org/10.1016/j.ceramint.2018.02.201
20. D. Gopi, J. Indira, L. Kavitha, M. Sekara and U. Kamachi Mudali, *Spectrochim. Acta A, Mol. Biomol. Spectrosc.*, **93**, 131 (2012); https://doi.org/10.1016/j.saa.2012.02.033
21. F. Vázquez-Hernández, C. Mendoza-Barrera, V. Altuzar, M. Meléndez-Lira and M.A. Santana-Aranda, *Mater. Sci. Eng. B*, **174**, 290 (2010); https://doi.org/10.1016/j.mseb.2010.03.011
22. J. Chen, Y. Wang, X. Chen, L. Ren, C. Lai, W. He and Q. Zhang, *Mater. Lett.*, **65**, 1923 (2011); https://doi.org/10.1016/j.matlet.2011.03.076
23. M.A. Giardina and M.A. Fanovich, *Ceram. Int.*, **36**, 1961 (2010); https://doi.org/10.1016/j.ceramint.2010.05.008
24. Z. Li, P. Wang and Z. Wu, *J. Mater. Sci.*, **40**, 6589 (2005); https://doi.org/10.1007/s10853-005-4222-7
25. S. Bose and S.K. Saha, *Chem. Mater.*, **15**, 4464 (2003); https://doi.org/10.1021/cm0303437
26. V.K. Mishra, S.K. Srivastava, B.P. Asthana and D.J. Kumar, *J. Am. Ceram. Soc.*, **95**, 2702 (2012); https://doi.org/10.1111/j.1551-2916.2012.05134.x
27. B. Nasiri-Tabrizi, P. Honarmandi, R. Ebrahimi-Kahrizsangi and P. Honarmandi, *Mater. Lett.*, **63**, 543 (2009); https://doi.org/10.1016/j.matlet.2008.11.030
28. J.M. Coelho, J.A. Moreira, A. Almeida and F.J. Monteiro, *J. Mater. Sci. Mater. Med.*, **21**, 2543 (2010); https://doi.org/10.1007/s10856-010-4122-5
29. K.S. Suslick, *Science*, **247**, 1439 (1990); https://doi.org/10.1126/science.247.4949.1439
30. K.S. Suslick, S.B. Choe, A.A. Cichowlas and M.W. Grinstaff, *Nature*, **353**, 414 (1991); https://doi.org/10.1038/353414a0
31. Y.C. Han, X.Y. Wang and S.P. Li, *Adv. Appl. Ceram.*, **108**, 400 (2009); https://doi.org/10.1179/174367609X414134
32. P. Rouhani, N. Taghavinia and S. Rouhani, *Ultrason. Sonochem.*, **17**, 853 (2010); https://doi.org/10.1016/j.ultsonch.2010.01.010
33. W. Kim and F. Saito, *Ultrason. Sonochem.*, **8**, 85 (2001); https://doi.org/10.1016/s1350-4177(00)00034-1
34. P.P. Wang, C.H. Li, H.Y. Gong, X.R. Jiang, H.Q. Wang and K.X. Li, *Powder Technol.*, **203**, 315 (2010); https://doi.org/10.1016/j.powtec.2010.05.023
35. F.Z. Huang, Y.H. Shen, A.J. Xie, J.M. Zhu, C.Y. Zhang, S.K. Li and J. Zhu, *J. Mater. Sci.*, **42**, 8599 (2007); https://doi.org/10.1007/s10853-007-1861-x
36. M. Snyder, P. Ng, H. Mekosh and P. Gagnon, *J. Sep. Sci.*, **32**, 4048 (2009); https://doi.org/10.1002/jssc.200900156
37. W. Pon-On, S. Meejoo and I.M. Tang, *Mater. Chem. Phys.*, **112**, 453 (2008); https://doi.org/10.1016/j.matchemphys.2008.05.082
38. M. Khalid, M. Mujahid, S. Amin, R.S. Rawat, A. Nusair and G.R. Deen, *Ceram. Int.*, **39**, 39 (2013); https://doi.org/10.1016/j.ceramint.2012.05.090
39. C. Garcia, C. Garcia and C. Paucar, *Inorg. Chem. Commun.*, **20**, 90 (2012); https://doi.org/10.1016/j.inoche.2012.02.024
40. W.J. Shih, M.C. Wang and M.H. Hon, *J. Cryst. Growth*, **275**, e2339 (2005); https://doi.org/10.1016/j.jcrysgro.2004.11.330
41. G.M. Cunniffe, F.J. O'Brien, S. Partap, T.J. Levingstone, K.T. Stanton and G.R. Dickson, *J. Biomed. Mater. Res.*, **95A**, 1142 (2010); https://doi.org/10.1002/jbm.a.32931
42. Y.S. Pan and D.S. Xiong, *J. Mater. Eng. Perform.*, **19**, 1037 (2010); https://doi.org/10.1007/s11665-009-9569-5
43. V.H. Nguyen, V.N. Thuy, T.V. Van, A.H. Dao and B.-J. Lee, *OpenNano*, **8**, 100064 (2022); https://doi.org/10.1016/j.onano.2022.100064
44. D. Bayraktar and A.C. Tas, *J. Eur. Ceram. Soc.*, **19**, 2573 (1999); https://doi.org/10.1016/S0955-2219(99)00132-6
45. M. Akram, R. Ahmed, I. Shakir, W.A.W. Ibrahim and R. Hussain, *J. Mater. Sci.*, **49**, 1475 (2014); https://doi.org/10.1007/s10853-013-7864-x
46. K.P. Sanosh, M.-C. Chu, A. Balakrishnan, Y.-J. Lee, T.N. Kim, S.-J. Cho, *Curr. Appl. Phys.*, **9**, 1459 (2009); https://doi.org/10.1016/j.cap.2009.03.024
47. A.L. Giraldo-Betancur, D.G. Espinosa-Arbelaez, A.d. Real-López, B.M. Millan-Malo, E.M. Rivera-Muñoz, E. Gutierrez-Cortez, P. Pineda-Gomez, S. Jimenez-Sandoval and M.E. Rodriguez-García, *Curr. Appl. Phys.*, **13**, 1383 (2013); https://doi.org/10.1016/j.cap.2013.04.019
48. S. Dasgupta, S.S. Banerjee, A. Bandyopadhyay and S. Bose, *Langmuir*, **26**, 4958 (2010); https://doi.org/10.1021/la903617e
49. A. Gozalian, A. Behnamghader, M. Daliri and A. Moshkforoush, *Sci. Iran.*, **18**, 1614 (2011); https://doi.org/10.1016/j.scient.2011.11.014
50. Y. Sasaki, S. Yamane, K. Kurosu, S.I. Sawada and K. Akiyoshi, *Polymers*, **4**, 1056 (2012); https://doi.org/10.3390/polym4021056
51. L. Pajchel and W. Kolodziejski, *J. Nanoparticle Res.*, **15**, 1868 (2013); https://doi.org/10.1007/s11051-013-1868-y
52. A. Zanotto, M.L. Saladino, D.C. Martino and E. Caponetti, *Adv. Nanopart.*, **1**, 21 (2012); https://doi.org/10.4236/anp.2012.13004
53. Z. Yang, Y. Jiang, L.X. Yu, B. Wen, F. Li, S. Sun and T. Hou, *J. Mater. Chem.*, **15**, 1807 (2005); https://doi.org/10.1039/B418015C
54. S.J. Gregg and K.S.W. Sing, Adsorption, Surface Area and Porosity, Academic Press: London, edn. 2 (1982).
55. G. Baskar, K. Lalitha, R. Aiswarya and R. Naveenkumar, *Mater. Sci. Eng. C*, **93**, 809 (2018); https://doi.org/10.1016/j.msec.2018.08.051
56. N. Al-Saran, P. Subash-Babu, D.M. Al-Nouri, H.A. Alfawaz and A.A. Alshatwi, *Environ. Toxicol. Pharmacol.*, **47**, 19 (2016); https://doi.org/10.1016/j.etap.2016.08.002
57. S. Srivastava, N. Kumar, R.S. Thakur and P. Roy, *Biol. Trace Elem. Res.*, **152**, 135 (2013); https://doi.org/10.1007/s12011-013-9602-2